Optical Lithography

Patrick Naulleau
Lawrence Berkeley National Laboratory, Berkeley, CA

1. Background

Optical lithography is a photon-based technique comprised of projecting, or shadow casting, an image into a photosensitive emulsion (photoresist) coated onto the substrate of choice. Today it is the most widely used lithography process in the manufacturing of nano-electronics by the semiconductor industry, a $200 Billion industry worldwide.

Optical lithography's ubiquitous use is a direct result of its highly parallel nature allowing vast amounts of information (i.e. patterns) to be transferred in a very short time. For example, considering the specification of a modern leading edge scanner (150 300-mm wafers per hour and 40-nm two-dimensional pattern resolution), the pixel throughput can be found to be approximately 1.8T pixels per second. This capability has arguably enabled the computing revolution we have undergone over the past 50 years.

Within the realm of optical lithography there exists a wide diversity of implementation both in wavelength and optical configuration. Wavelengths range from the traditional visible and ultraviolet ranges down to extreme ultraviolet (EUV) and even soft X-ray. Optical configurations range from the simplest case of direct shadow casting to complex multi-element refractive and/or reflective imaging systems. Additionally, diffractive systems can be used for applications such interference and scanning probe lithography.

1.1 History

The earliest optical lithography tools used in the manufacturing of semiconductor devices were of a type classified at contact printers. In these systems, a mask is placed in direct contact with the photoresist-coated wafer and light is shined through the mask. Patterned areas on the mask served to block the light causing the negative of the pattern to be transferred to the wafer. The problem with the contact approach, however, was the rapid generation of defects on the mask, which are subsequently replicated in all exposures. The industry addressed this problem with the introduction of proximity lithography which is essentially the same as contact lithography but with a small air gap maintained between the surface of the mask and the wafer. This mitigated the defect problem but at the cost of resolution limitations arising from diffraction, or spreading of the light, upon propagation of the light through the free-space gap between the mask and wafer.

The free-space diffraction problem was eventually solved by introducing an imaging system between the mask and the wafer. The gap can now effectively be eliminated since the function of the imaging system is to replicate the electric field present in its object plane to its image plane. Any focus error in this optical system can be thought of simply as equivalent to the gap present in the proximity tool with the further benefit of allowing the gap to effectively become negative thereby expanding the acceptable gap or focus operating range. In addition to solving the proximity diffraction problem, using an imaging system enables demagnification from the mask to the wafer. This is beneficial since it greatly relaxes mask requirements both in terms of feature quality and defects. The demagnification cannot be made too large, however, since mask size would become an issue. Modern projection optical lithography tools use a demagnification of 4.

1.2 Today's Optical Lithography Tools

Projection lithography tools now come in two variations: step and repeat, and step and scan. In the step and repeat system (a stepper) the entire mask is illuminated and projected onto the wafer exposing one "die" (approximately 25 mm × 25 mm in size at the wafer). The light is then turned off and the wafer shifted (stepped) and the exposure process repeated. This cycle is continued until the entire wafer is exposed. In a step and scan system (a scanner) the imaging field size is reduced to a slit (typically on the order of 6 mm × 25 mm at the wafer) greatly facilitating the design and fabrication of the optical system. The mask and wafer stages are then scanned in opposite directions at the proper speeds such that the entire mask pattern is replicated in one scan again creating an exposed die this time with a typical size of approximately 25 mm × 32 mm at the wafer. As with the stepper, the light is then turned off and the wafer shifted over to an unexposed region where the die scan process is repeated.

Since the advent of the scanner, further changes/improvements to the technology have come in the form of increases in numerical aperture, decreases in wavelength, and the introduction of immersion fluids between the projection optic and the wafer. One of the most significant developments currently underway is the reduction of the wavelength from 193 nm to 13.5 nm. This quantum leap in wavelength comes with many additional changes including high vacuum operation and the requirement for all reflective components including both the optics and the mask. Reflective imaging systems, however, are not new to lithography; in fact many of the earliest systems were based on reflective optics due to their achromatic characteristics which was crucial before line-narrowed lasers were developed.

It is interesting to note that while contact lithography represents the dawn of the technology, one could argue that it has made a resurgence on the form of nano-imprint lithography. Nano-imprint uses direct contact between the mask and the wafer and for the case of "step and flash" light is shined though the mask to "cure" the resist. The difference, however, is that the light itself does not transport the pattern but rather simply cross-links the photoresist material. It is the mask that transports the pattern by physically displacing the photoresist in the patterned area before cross-linking. For this reason, unlike any of the optical lithography methods described above, the illumination wavelength has no effect on the resolution of the process. Thus, although the nano-imprint process does use photons, we do not classify it as an optical lithography technique.

The topic of optical lithography is by far too vast to be cover in one small chapter. The goal here is simply to provide an introduction of the topic with the hope of making the reader aware of the various optical lithography options available, as well as to provide some basic understanding of the capabilities and limits of the technology. Since resolution is typically of paramount concern for nanofabrication, an attempt is made to provide a fundamental understanding of resolution limits and depth of focus in various optical systems. Next the issue of coherence is addressed, and again with particular focus on resolution and depth of focus. Finally the future of optical lithography is explored, ending with a brief discussion of practical considerations for lab-based use. For much more detailed discussions of optical lithography, the reader is referred to several exhaustive texts on the topic [1-3].

2. Resolution

Wavelength is the fundamental limiting factor in determining the resolution of optical lithography systems. However, wavelength alone does not provide the entire picture, also crucial to understanding resolution limits in optical lithography systems is the concept of diffraction. Diffraction occurs as light is passed through a limiting aperture. Although beyond the scope of this chapter, the phenomenon of diffraction can be readily predicted using Maxwell's equations and heuristically explained using Huygen's Principle, which itself can be derived from Maxwell's equations [4, 5]. Using these techniques

one can show that the diffraction half angle θ introduced to a plane wave of wavelength λ upon propagation through an aperture of width *W* is

$$\theta = \text{asin}(\lambda/W). \qquad (6.1)$$

Figure 6.1 shows an example of the diffraction process where we assume a wavelength of 13.5 nm and a slit aperture size of 300 nm with propagation distances up to 25 μm. The spread of the beam is clearly observed.

The aforementioned simple diffraction equation presented above can be directly applied to predict the maximum allowable gap in a proximity lithography tool. Given a target resolution *W*, and a wavelength λ, and setting the maximum allowable diffraction blur to be equal to the target resolution, the required gap *L* can be written as

$$L = W\sqrt{\frac{W^2}{\lambda^2} - 1}\,. \qquad (6.2)$$

Given a target resolution of 50 nm and a wavelength of 13.5 nm, the gap would have to be smaller than 178 nm.

Although the aforementioned diffraction equation is also directly responsible for the resolution limit of an imaging lithography tool, the connection is less evident. In heuristically understanding the relationship between resolution and diffraction in this case, it is useful to think of the lens as a component that simply inverts the diffraction caused by the mask. Taking for granted that the propagation of light is reversible, to produce an image of an aperture of width *W* at some wavelength λ, we are required to generate a converging

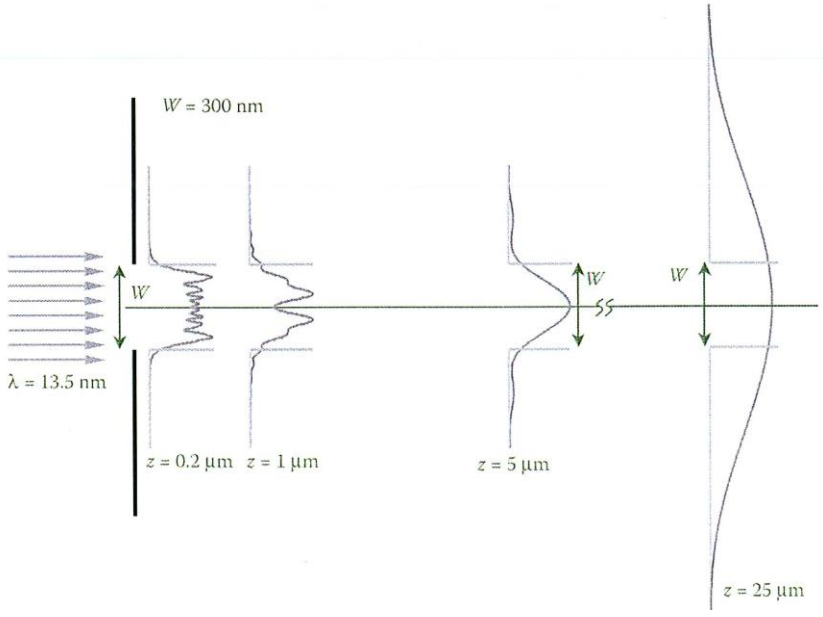

Figure 6.1 Example of the diffraction process where we assume a wavelength of 13.5 nm and a slit aperture size of 300 nm with propagation distances of up to 25 μm.

wave where the convergence angle is simply equal to the divergence angle that would be produced upon diffraction in the forward case. Thus the minimum image size a lens can produce depends on the range of input angles that can be inverted by the lens and the wavelength,

$$W = \lambda/\sin(\theta_c) \qquad (6.3)$$

where θ_c is the maximum half angle accepted by the lens. The *sine* of the collection half angle (assuming a medium index of unity) is referred to as the numerical aperture (NA) of the lens allowing the minimum feature size equation to be rewritten as

$$W = \lambda/\mathrm{NA}. \qquad (6.4)$$

It is important to note that the magnification has been assumed to be unity in the discussion here. Typical lithography optics are demagnifying and we are generally interested in the resolution on the image side (unlike microscopy systems), thus the NA of interest is the image side-NA rather than the acceptance NA. The two, however, are simply related by the magnification. For example, a so called 4× lithography system, which demagnifies the object by a factor of 4 will have an image-side NA that is 4 times larger than the object-side NA.

Using the image-side NA, Equation 6.4 now can be thought of representing the resolution limit of the projection tool. The problem with this interpretation, however, is that Equation 6.4 is based on a subjective definition of the diffraction half-angle used in Equation. 1. Although not explicitly stated here, the angle in Equation 6.1 was chosen to correspond to the point of the first null in the diffraction pattern. While arguably reasonable, there are certainly various other metrics that could be used to define this angle: for example the angle at which the diffraction intensity is half maximum or 1/e. The definition of resolution is thus subjective, and in practice, depends on a variety of factors including but not limited to illumination conditions, characteristics of the object (mask), the signal to noise ratio, capabilities of the detector (photoresist), and so on. To account for this subjective nature, the resolution of lithography systems is typically defined as

$$R = k_1\, \lambda/\mathrm{NA} \qquad (6.5)$$

where k_1 is the process dependent resolution factor. From the optical perspective and considering periodic structures, physics can be shown to set the lower limit of k_1 to 0.25. For isolated structures of relatively loose pitch, however, the ultimate limitation of what can be printed depends more on the process than the optics. Thus, effective k_1 factors of smaller than 0.25 can be achieved. Examples of this are now routine in the IC industry, for example, 22-nm devices will be commercialized in the near future using 193-nm lithography. Assuming a numerical aperture of 1.35 (the highest currently available) this would correspond to a k_1 factor of 0.15.

Given the definition of NA presented here, one might ask how it is possible to achieve an NA that is greater than unity. The answer to this apparent dilemma is that we had assumed a medium index of unity. The complete definition of NA is in fact

$$\mathrm{NA} = n \sin(\theta) \qquad (6.6)$$

where n is the index of refraction of the medium between the lens and the image plane. This fact has long been used by microscopists in the form of oil-immersion lenses. The IC industry has recently adapted this technology to produce water immersion lithography tools [6,7] with NAs of up to 1.35. In principle even higher NA tools could be developed; however, materials issues have halted progress on

that front [8]. Heuristically, it is instructive consider the NA to be defined with an n of unity and instead note that the effective wavelength in the medium is λ/n, where λ is the vacuum wavelength From this perspective, we see that what takes place is an effective reduction in wavelength rather than a change in the actual collection angles.

The exact same analysis used to determine the resolution of imaging lithography systems can also be applied to optical scanning probe systems such as zone plate array lithography (ZPAL) [9]. This is because in some sense these are in fact imaging systems with the object being restricted to a single point. The main drawback of scanning systems is that they are extremely slow since they do not make use of the intrinsic massive parallelism enabled by optical systems. This problem can be mitigated, however, by using an array of probes as is done in ZPAL. Although not a requisite for scanning probe systems, ZPAL uses Fresnel zone plate (diffractive) optics for simplicity and cost. Using such optics for large field systems is not feasible due to their extremely small field of view. As with the conventional optics discussed hitherto, the resolution of diffractive optics can also be characterized by the NA. Although beyond the scope of this chapter, it can also be shown that the resolution limit of a diffractive lens is simply defined by the size of the smallest zone width on the lens [10]. This should not be a surprise since the zone width will determine the converging diffraction angle.

Another important class of optical lithography tools, especially for lab use, is the interference tool, where two mutually coherent beams are combined at an angle (Figure 6.2). The mechanism used to create the two beams can vary and includes refractive, diffractive, and reflective methods. Ultimately, all that matters is the combining angle and the wavelength. Using Fourier Optics [4], a plane wave traveling at some angle can be expressed by its spatial frequency

$$f_x = \sin(\theta)/\lambda. \qquad (6.7)$$

As shown in Figure 6.2, the interfering frequency becomes the difference between the two or 2 f_x. From the perspective of resolution, it is instructive to instead consider one half the period of the interference term. The interference pattern period (T) and resolution can be written as

$$T = 1/(2f_x) = \tfrac{1}{2}\,\lambda/\sin(\theta) \qquad (6.8a)$$

$$R = \tfrac{1}{2}\,T = \tfrac{1}{4}\,\lambda/\sin(\theta) \qquad (6.8b)$$

Maximum resolution is achieved when the interfering beams travel in opposite directions ($\theta = 90°$), enabling the patterning of $\lambda/4$ features, not coincidently matching the $k_1 = 0.25$ limit discussed here. In addition, immersion methods can be used to further push the resolution by reducing the effective wavelength [11].

In the aforementioned resolution discussions above, the implicit assumption was made that the image is observed at the ideal focal plane. In practice, however, it may be difficult to maintain the wafer in that ideal plane and even more fundamentally, the photoresist being imaged into will have some finite thickness. Consequently, the longitudinal distance over which the resolution of an optical system is preserved, or its depth of focus (DOF) becomes extremely important. In practical terms, the DOF can be defined as the longitudinal distance over which the change in size of a single image point is less than or equal to the minimum size of the image point as set by the diffraction limit discussed above.

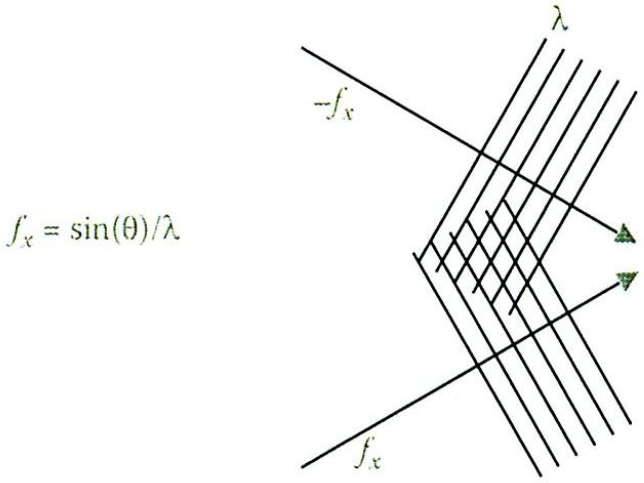

Figure 6.2 Schematic of a lithographic interference tool where two mutually coherent beams are combined at an angle.

We again begin by considering the simple proximity lithography case. Recall that when determining the maximum allowable gap, as described here, a similar criterion was used requiring the diffraction blur to be less than or equal to the actual feature size on the mask. Thus one can think of this maximum gap (Equation 6.2) as being equivalent to the DOF since mechanical constraints limit the minimum size of the gap to 0.

For projection systems (refractive, reflective, and/or diffractive), the DOF can be elucidated with simple geometry (Figure 6.3). Using geometric optics, the single-sided blur as a function of defocus (d) can be expressed as

$$\text{Blur} = d\ \text{NA}. \tag{6.9}$$

Setting the maximum allowable blur to be equal to the resolution limit of the system yields

$$\text{Blur}_{\text{max}} = d_{\text{max}}\ \text{NA} = \lambda/\text{NA}. \tag{6.10}$$

Now solving for d_{max} yields

$$d_{\text{max}} = \lambda/\text{NA}^2 \tag{6.11}$$

Again applying a process-dependent factor, the DOF becomes

$$\text{DOF} = k_2\ \lambda/\text{NA}^2, \tag{6.12}$$

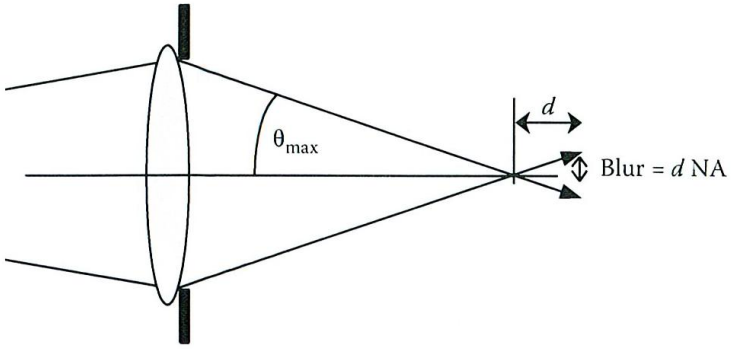

Figure 6.3 Schematic describing the geometry leading to depth of focus limits in optical systems.

where k_2, similar to k_1, is a constant representative of the lithographic process conditions. A typical value for k_2 for a conventional process is 0.5.

Turning to interference tools (Figure 6.2), and again assuming full spatial coherence (coherence issues will be discussed in more detail in the next section 6.3), it is evident that the generated interference will be independent of longitudinal position. Thus, in an ideal interference tool the DOF is effectively infinite. In practice, however, the DOF in the perfect coherence case will be limited by the finite overlapping footprint of the two interfering beams. Since the two beams are crossing each other as shown in Figure 6.2, this overlapping footprint will be maximized at only one longitudinal point and will decrease linearly from that point in either direction. This constraint, however, is certainly not very restrictive and can be represented mathematically as

$$\mathrm{DOF} = D/[2\tan(\theta)], \qquad (6.13)$$

where D is the beam diameter and 2θ is the angle between the two interfering beams.

In conclusion, it is noted that alternative and certainly more complete discussions of resolution and depth of focus can be found in the literature [4,5,12].

3. Coherence

Although not explicitly addressed in the discussions so far, illumination coherence plays an important role in the achievable resolution/DOF of optical systems. However, by and large, modern day steppers employ extremely narrowband sources allowing temporal coherence effects to be ignored leaving only spatial coherence. As discussed later, the exception to this are diffractive methods in which case temporal coherence can play an important role. Detailed discussions of coherence theory in general can be found in the literature [5,13]. In the parlance of lithography, coherence is almost universally described in terms of the partial coherence factor or σ. Most fundamentally, σ can be thought of as the ratio of the diffraction-limited resolution to the coherence width. When the coherence width is larger than the resolution limit, σ is <1. In most practical cases, σ is <1 and typically falls in the range of 0.2 to 0.8, with 0.2 being close to coherent and 0.8 being close to incoherent.

Implicit in the definition discussed earlier is the assumption that the concept of coherence width is understood, thus it is quickly reviewed here. In a practical sense, coherence width is best explained by recalling Young's double-slit experiment (Figure 6.4). In this experiment, two small apertures are placed

in the optical beam and the contrast of the interference pattern created in the region where the two diffracted waves overlap is observed. As the separation between the two apertures goes to zero it is evident that the diffracted beams will become fully correlated (mutually coherent) since they are emanating from the same point and thus will interfere with high contrast. In general, as the separation is increased, the correlation will decrease and so will the interference contrast. The coherence width can be defined as the separation between the two apertures where the interference contrast drops to 50%.

A basic understanding of the effect of coherence on imaging performance is perhaps best achieved from the perspective of the optical system transfer function [4]. Given a unity contrast sinusoidal object, the transfer function describes the contrast of the resulting sinusoidal image for all possible frequencies. For illustrative purposes, Figure 6.5 shows the transfer function of an ideal projection system for three difference values of σ: 0.1, 0.5, and 1. The frequency axis in Figure 6.5 is normalized to λ/NA which represents the coherent cutoff of the system. The plot shows that, in terms of ultimate resolution capabilities, larger values of σ are preferable, but they come at the cost of performance at more moderate feature sizes. It is important to note these results assume on axis illumination and a pure amplitude mask; letting these variables float can significantly change the results allowing the imaging performance to be optimized for specific feature types. These technologies are generally referred to as resolution enhancement techniques. Although beyond the scope of this chapter, detailed information on this topic can be found in Refs. [1,2]. In addition to effecting resolution, these various parameters also have significant impact on DOF. It is important to note that these techniques do not change the fundamental resolution limits set by λ and NA but rather provide a mechanism for reducing k_1 and/or k_2.

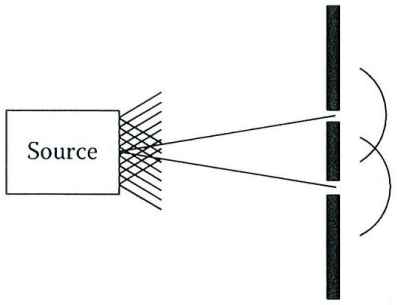

Figure 6.4 Schematic depiction of Young's double-slit experiment.

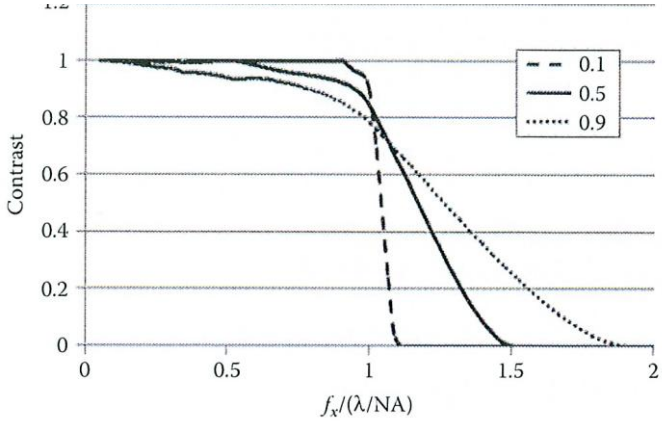

Figure 6.5 Transfer function of an ideal projection system for three difference values of σ: 0.1, 0.5, and 1. The frequency axis is normalized to λ/NA which represents the coherent cutoff of the system.

As mentioned in the previous section, coherence plays an important role in the determination of DOF for interference lithography systems. In that scenario, the concept of partial coherence factor is less useful. More insight can be gained by instead using the un-normalized coherence width W_c. The requirement for DOF now becomes that the shear (lateral displacement) between the two interfering waves be smaller than W_c. Determining the shear depends on the type of interference tool being used, wavefront or amplitude division. Examples of the two different types (both based on gratings) are shown in Figure 6.6. In wavefront division, very large coherence width is required since by design, the two interfering beams are extracted from different lateral locations in the incident wavefront. The coherence width is required to be significantly larger than the total printed width and thus W_c plays little role in the DOF. Rather the DOF is determined by the coherent equation that is, Equation 6.13.

Amplitude division, on the other hand, can be applied in cases where there is significantly less coherence because full copies of the input wavefront are created and then recombined allowing zero shear to be obtained at the cross-over point. As the beams propagate away from the cross-over point,

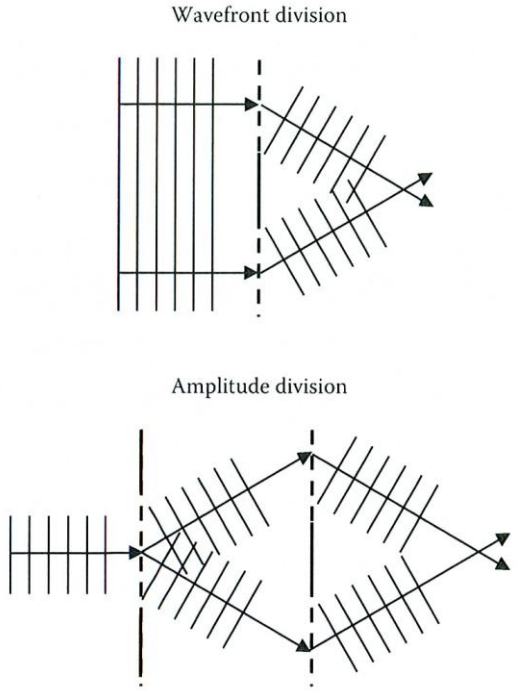

Figure 6.6 Schematics depicting the distinctions between wavefront and amplitude division interference tools.

a shear is introduced that is directly proportional to the interference angle. In such a system, the DOF can be shown to be

$$\mathrm{DOF} = W_c / [2 \tan(\theta)], \qquad (6.14)$$

where 2θ is again the angle between the two interfering beams.

Finally, the lateral coherence (W_c) itself is considered. Although a full discussion of this vast topic is certainly beyond the scope of this chapter, valuable insight can be gained by considering a simple limiting case. The simple case we consider is a fully incoherent source that is re-imaged to the entrance

plane of our system, be it the mask in a projection lithography tool or the beamsplitter in an interference tool. The optic used to re-image the source is often referred to as the "condenser" and such an illumination system is commonly referred to as "critical" [13] (Figure 6.7). In this case the coherence width is simply determined by the resolution of the condenser lens. Heuristically this can be explained by noting that source variations, which lead to incoherence, that are finer than the condenser resolution cannot be reproduced.

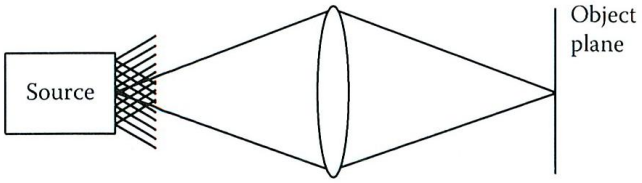

Figure 6.7 Schematic of a "critical" illumination system.

Thus, mathematically we can express the coherence width in this case as

$$W_c = \lambda/\mathrm{NA_c} \qquad (6.15)$$

where $\mathrm{NA_c}$ is the image-side NA of the condenser lens. Having defined σ as the ratio of the resolution to the coherence width, we see that for a critical illuminator, σ simply becomes the ratio of the condenser NA to the object side imaging NA.

$$\sigma = \mathrm{NA_c}/\mathrm{NA_o}. \qquad (6.16)$$

Although temporal coherence, or bandwidth, plays an insignificant role in the imaging performance of modern projection lithography tools, one needs to be aware of its impact on diffraction- based and interference tools. First it is instructive to consider the relationship between temporal coherence and bandwidth. The Wiener–Khinchin theorem [13] teaches us that there exists a Fourier transform relationship between the two. Thus, to first order, the coherence time becomes the inverse of the bandwidth, making short temporal coherence equivalent to large bandwidth. This is important because the effect of bandwidth on a system is much easier to visualize than the effect of temporal coherence.

Beginning with the diffraction-based zoneplate system such as ZPAL, the highly chromatic nature of the Fresnel zoneplate makes bandwidth a concern. The focal length of a zoneplate can be shown to be [10]

$$f \approx D\,\Delta r / \lambda, \qquad (6.17)$$

where D is the diameter and Δr is the outer zone width. The focal length is inversely proportional to the wavelength, thus resolution will be adversely affected by increased bandwidth. From Equation 6.17 the change in focal length as a function of bandwidth, $\Delta\lambda$, can be written as

$$\Delta f = \Delta\lambda\, D\, \Delta r / \bar{\lambda}^2, \qquad (6.18)$$

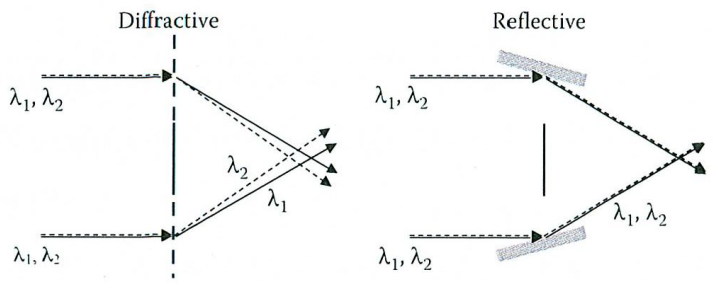

Figure 6.8 Schematics of reflective and diffractive beam combiners as could be used in interference lithography tools.

where $\bar{\lambda}$ is the mean wavelength. Using Equation 6.10 to determine the resolution based on a defocus of ½ Δf (the single sided focal change) the resolution can now be expressed as

$$R = \frac{\Delta\lambda}{\bar{\lambda}} \frac{D}{4}. \qquad (6.19)$$

Conversely, when considering interference tools, diffractive properties are in fact beneficial in terms of to tolerance to bandwidth. This can be explained with the help of Figure 8 showing both reflective and diffractive beam combiner cases. For simplicity, wavefront division and spatial coherence are assumed. In the diffractive case, the longer wavelength (λ_2) is bent more. The frequency of the interference fringes produced will then depend on the angle of interference and the wavelength. It can be shown that the increased diffraction angle is exactly balanced by the increased wavelength to produce the identical frequency fringes as are produced by λ_1. Thus, the system can produce high quality fringes with broadband light. In the reflective system, on the other hand, the interference angles are identical for both wavelengths owing to the achromatic nature of reflection. This causes the two different wavelengths to produce fringes of two different frequencies thereby in sum generating poor quality fringes in the presence of broadband light. The tolerable bandwidth depends on the lateral range over which one desires to produce high contrast fringes [13].

4. Pushing the limits of optical lithography

Modern developments in optical lithography are now enabling this technology to approach resolutions previously only capable with much slower e-beam methods. Unlike in the past, recent improvements on the manufacturing floor have not come as a benefit of reduced wavelength. The last attempt to change wavelength was the shift to 157 nm which was abandoned due to the birefringence problem. Currently, leading edge industry is still operating at a wavelength of 193 nm but as described in the resolution section the numerical aperture has been increased to beyond unity using an immersion process akin to oil-immersion microscopy.

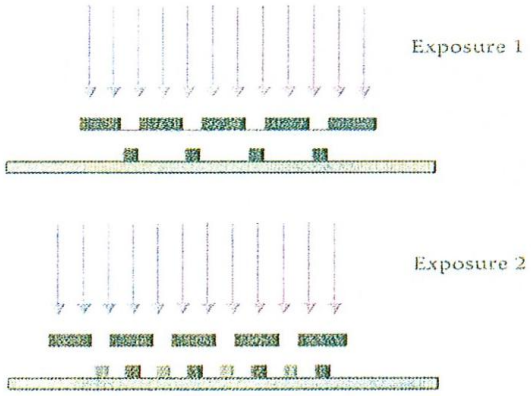

Figure 6.9 Schematic depicting a double-patterning process.

An alternative of the immersion process is to keep the numerical aperture fixed and define the effective wavelength as the vacuum wavelength divided by the index of the medium. At a wavelength of 193 nm, the refractive index of water is n_w = 1.437, thus water immersion can be used to operate at an effective wavelength of 134 nm. This wavelength corresponds to a single exposure periodic structure resolution limit of 33.5 nm.

The key qualifiers in the resolution limit are "single exposure" and "periodic". Industry has recently been pushing beyond even this limit using a concept that can simply be described as interlacing. Referred to by the industry as "double patterning", these techniques rely on printing at a looser pitch and then shifting and printing again thereby decreasing the effective pitch as shown in Figure 6.9. The process works because optical systems fundamentally limit pitch and not isolated feature size. The "size" of an isolated feature after going through a threshold process (which ideally is what a photoresist does) is determined by the threshold level and can become arbitrarily small, ultimately being

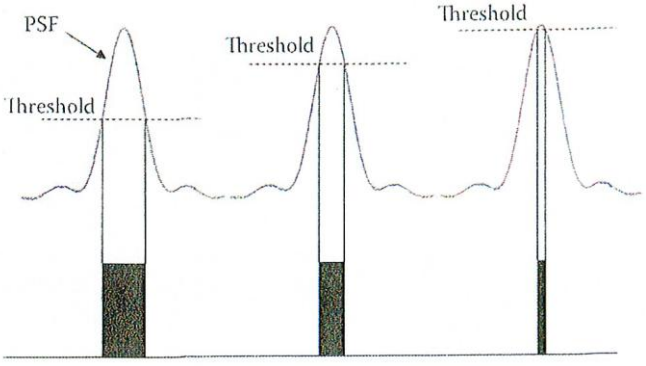

Figure 6.10 Schematic showing how dose can be used to shrink feature size at a fixed pitch apparently circumventing the λ/NA limit, but only for isolated

limited by noise and process control. Traditional resolution descriptions of isolated features are

determined by the width of the point-spread function (PSF) which is customarily defined as the full width at half-maximum. Thus the definition assumed a threshold value of 50%, but as we allow the threshold to get higher and higher, the feature width becomes ever smaller (Figure 6.10). Although it is fine for isolated features, such a process cannot arbitrarily shrink the minimum resolvable separation between two features, thus the need for double patterning.

The aforementioned simplified description represents only one of the many potential double patterning approaches including an approach called “spacer” [14] requiring only a single exposure and relying on processing to double the pattern density. In principle, these methods can be extended beyond double patterning to triple and even more to further push down feature sizes. However, even double patterning comes at a prohibitive cost compared to single exposure methods raising concerns about the commercial viability of extending these techniques to triple and more.

5. Taking optical lithography to the extreme

The escalating costs and difficulties associated with subquarter-wavelength lithography using double patterning and beyond provide great impetus for the return of a viable single patterning optical technique. As shown in section 6.2, the only way to drive the optical resolution down in terms of half pitch is to increase the NA and/or decrease the wavelength. As mentioned here, increases in NA have been pushed to the limit and are now constrained by the availability of adequate high-index materials. Materials limitations in terms of suitable high-quality low birefringence glass have also put an end to wavelength reduction, at least for refractive systems. For wavelength reduction, however, one can turn to reflective optics to get around the materials issues, but reflective solutions come with restrictions in NA due geometric limitations. The NA restrictions, however, are readily overcome through even greater reductions in wavelength.

This train of thought has led to the development of extreme ultraviolet (EUV) lithography which relies on a wavelength of 13.5 nm. The 14× reduction in wavelength from 193 nm to 13.5 nm will be the largest single wavelength shrink in the history of modern optical lithography as applied to microelectronics fabrication. This significant jump in wavelength affords the additional benefits of small numerical apertures and large operational k_1 factors. These associated benefits lead to the very important manifestations of long extendibility of the technology and large DOF.

At its core, EUV lithography is indeed simply an extension of optical lithography. All the concepts presented up to this point in this chapter remain directly applicable to EUV. The difference in implementation is simply that we now rely on reflective components for both the mask and the imaging optics instead of refractive. Figure 6.11 schematically depicts the reflective EUV configuration in a much simplified implementation. It should be noted that the use of reflective optics is not a fundamental concern since such optics have long been utilized in the ultraviolet and deep ultraviolet lithography regime in the form of catadioptric exposure lenses [15-18]. In addition to the obvious change to all reflective components, geometry requires the mask to be tilted and the light to come in at an angle compared to the on-axis condition for the transmission case. The angle of the mask is readily compensated for by also tilting the wafer at an angle that is scaled down by the magnification of the optical system. A more subtle impact of the mask tilt and the three-dimensional nature of the absorber

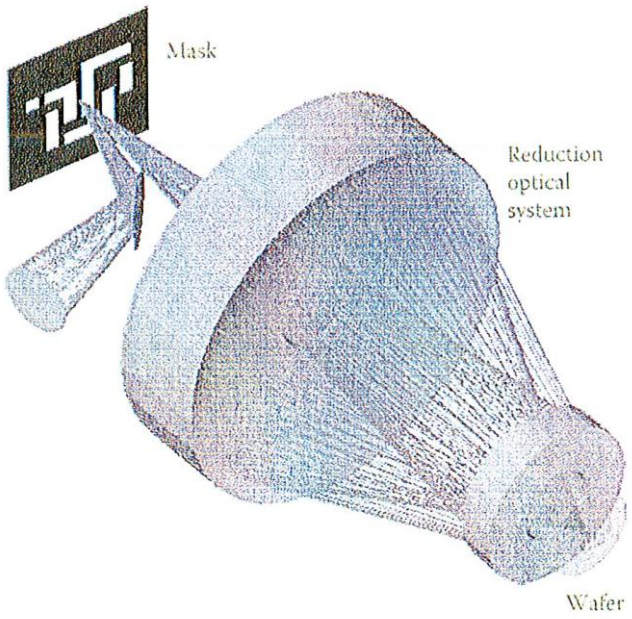

Figure 6.11 Schematic depiction the reflective lithography configuration required at EUV wavelengths.

structure on the mask is that shadowing occurs on the lines running perpendicular to the direction of the illumination which in turn leads to an effective shrinking of the lines in the image. This effect, however, can be compensated through proper biasing of the features during fabrication of the mask.

5.1. EUV-specific challenges

5.1.1. Multilayers

Although simply an extension of optical lithography, EUV lithography certainly comes with its own set of challenges. First, obtaining high reflectivity in the EUV wavelength regime is not trivial. The development of EUV lithography has been enabled by the invention of high reflectivity near-normal incidence Bragg coatings [19] allowing high NA EUV optics with reasonable throughputs to be fabricated. One such coating is the Molybdenum-Silicon multilayer providing peak reflectivity near 13.5 nm. It is typically comprised of 40 bilayers with a bilayer thickness of approximately 7 nm. This coating now serves as the basis for all EUV lithography optics. Although tremendous improvements have been made in this area allowing near-theoretical limit reflectivities to be achieved on a routine basis, the theoretical limit is only 70%. This relatively low reflectivity places significant constraints on the number of mirrors that can be used in both the illuminator used to transport and shape the light from the source to the mask as well as in the imaging optic itself. Current manufacturing class EUV tools operating at 0.25 NA utilize 6 mirrors in the imaging system and approximately four in the illuminator. Further adding the mask, a typical tool might have 11 multilayer surfaces which in the ideal case would give you a total reflectivity of 2%. If reduction in bandwidth is also considered, one can find the effective throughput of the tool to shrink even faster as mirrors are added.

5.1.2. Source

In addition to putting constraints on the optical design, the throughput issue places higher demands on source power and source power has long been viewed as the biggest challenge facing EUV. Current lithography tools use high power excimer lasers, however, direct scaling of laser technology to EUV wavelengths is not feasible from the perspective of use in exposure tools. Two major classes of sources are under development for use in production scale EUV exposure tool: laser-produced [20,21] and discharge-produced [22] plasmas. Not only must EUV sources produce high power, but they must do it in a clean manner making debris mitigation another crucial issue for the source. High-power EUV sources typically generate large amounts of energetic debris which if allowed to strike mirrors will quickly deteriorate them. Various methods exist for controlling debris [23-28]. It is important to note that debris mitigation typically comes at the cost of optical throughput and thus is an important consideration in tool design. Despite these challenges, tremendous improvements have been made on both types of sources allowing good results to be obtained from alpha tools and supporting pilot tool operation in the near future.

5.1.3. Vacuum

Because EUV light is strongly absorbed by all materials, including atmosphere, EUV systems operate under high vacuum. Moreover, the purity of the vacuum is also crucial due to the fact that the high energy of the EUV photons has the ability to dissociate molecules leading to contamination of optical surfaces and subsequent loss of reflectivity. One common potential source of contamination is residual hydrocarbon in the vacuum. Hydrocarbons dissociated by the EUV radiation are highly reactive and lead to carbon growth on the multilayer surfaces. A 1% loss in reflectivity requires only 0.8-nm of carbon growth. For a system with a total of nine multilayer reflections, such contamination would lead to a throughput loss of 10%. Carbon contamination, however, is generally accepted to be a reversible process. Oxidation of multilayers is another potential problem. This can occur when oxygen containing molecules, such as water, are split into radicals by means of photoemission leading to oxidation of the multilayer surface and again reflectivity loss. Oxidation is of greater concern than carbon growth because its reversal is considerably more complicated [29].

5.1.4. Mask defects

As noted earlier, in EUV lithography the mask must also be reflective. The most daunting challenge this reflective architecture poses to the mask is the possibility of defects embedded underneath or within the multilayer stack. If these embedded defects lead to surface indentations on the order of 3 nm or even smaller, they will act as strong phase-shifting defects with potentially considerable impact on the printed image. The detection, mitigation, and repair of such defects is a crucial engineering challenge facing the commercialization of EUV lithography.

5.1.5. Flare

Another issue particularly relevant to EUV is flare. Flare in optical systems in general is simply scattered light leading to a DC background in the image and subsequent loss of contrast. The only major contributor to flare in EUV systems is projection optics roughness and the resulting scatter [30]. EUV lithography's short wavelength renders it very vulnerable to surface roughness. Although atomic-level long range accuracy as required for wavefront control is now readily achieved [31], such precision cannot be obtained at the shorter spatial scales relevant to flare. Early EUV production tools are expected to have flare levels on the order of 10% with potentially significant variations across the field. The resulting CD variation, however, can be controlled using mask-based flare compensation techniques [32-33].

5.2. From the lab to the factory

EUV lithography has been in development since the mid-1980s but has recently entered the early manufacturing integration study phase [34-36]. Currently operational are full field "alpha" tools with NAs of 0.25 [37-39] and microfield exposure tools with NAs of 0.3 [40-43]. Assuming a k_1 factor of 0.4, the corresponding half-pitch resolution limits are 22 nm and 18 nm for these two sets of tools, respectively. Figure 6.12 shows recent results from the SEMATECH Berkeley Microfield Exposure Tool used for advanced development of resists, processes, and masks.

The next phase in commercialization will be the deployment of so called "pilot line" tools used to establish high volume manufacturing processes. These tools are currently under development and slated to be delivered to several key integrated circuit manufacturers [44]. As with the alpha tools, the pilot tools will also have an NA of 0.25, however, the first production tools are expected to have NAs of approximately 0.32 being suitable for half pitches down to 16 nm. As with conventional optical lithography systems in the past, extension to even finer resolutions in the future is expected with increasing NA and decreasing wavelength. Designs with NAs of up to 0.7 have been presented [45] as well as multilayers with reflectivities of 41% at 6.8 nm wavelength [46]. Using these parameters and an assumed k_1 limit of 0.25, EUV would be extendable to a half pitch resolution of 2.4 nm.

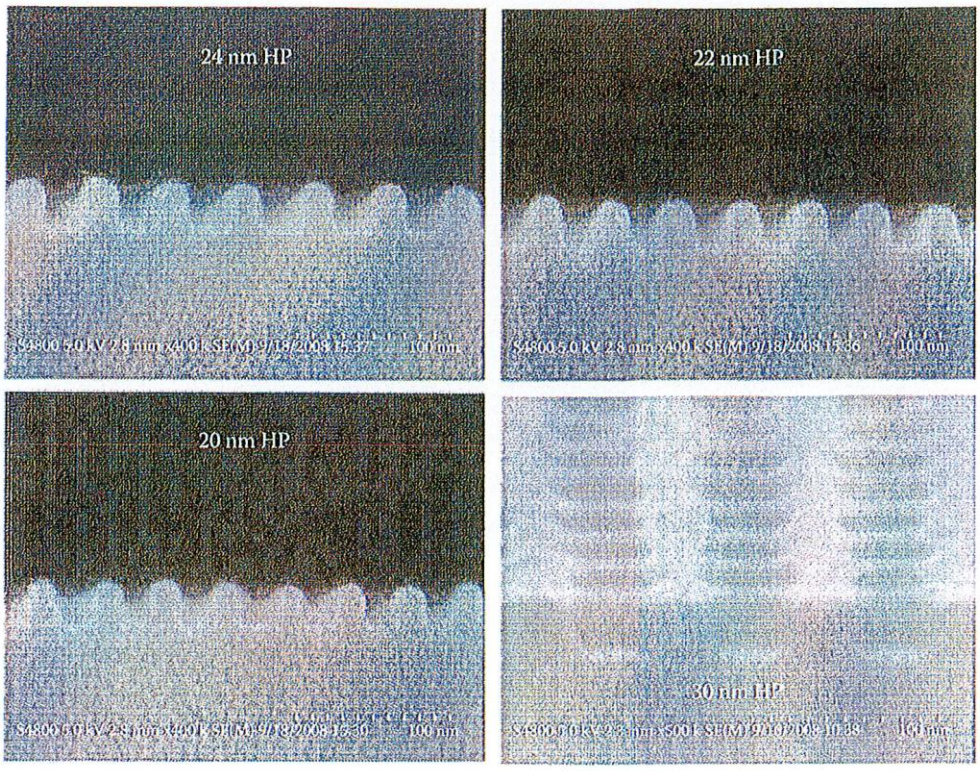

Figure 6.12 Recent results from the SEMATECH Berkeley Microfield Exposure Tool showing patterning capability down to 20 nm lines and spaces and 30 nm contacts.

6. Practical considerations for lab-based nanofabrication

While arguably the most widely used and highest throughput lithography technique for patterning of nanostructures, leading edge optical lithography is not particularly well suited for low volume lab-based applications. This is due to the extremely high capital cost of leading edge tools and masks. Nevertheless, optical lithography can play an important role in this regime. For example, older

generation depreciated and/or contact lithography tools could be used in conjunction with slower high resolution methods such as e-beam to pattern large area "support" structures, alleviating write time burden on the e-beam tool.

In terms of actually using optical lithography for very fine patterns, if access to projection tools is available one must also be aware of mask requirements both in terms of lead time and costs. If needs are limited to strictly periodic structures, either lines or contacts, interference lithography is an excellent option. Interference lithography can also be combined with other lithography techniques, optical or otherwise, to customize the periodic pattern for the generation of more complex structures.

6. References

1. H. J. Levinson, *Principle of Lithography,* Second Edition, SPIE Press, Bellingham, Washington, 2005.
2. C. Mack, *Fundamental Principles of Optical Lithography: The Science of Microfabrication*, Wiley-Interscience, New York, 2007.
3. K Suzuki, B. W. Smith, *Microlithography: Science and Technology,* Second Edition, CRC Press, Boca Raton, Florida, 2007.
4. J. W. Goodman, *Introduction to Fourier Optics*, Second Edition, McGraw-Hill, New York, 1996.
5. M. Born and E. Wolf, *Principles of Optics: Electromagnetic Theory of Propagation, Interference and Diffraction of Light*, Seventh Edition, Cambridge University Press, Cambridge; New York, 1999.
6. Hiroaki Kawata, James M. Carter, Anthony Yen, and Henry I. Smith "Optical projection lithography using lenses with numerical apertures greater than unity," Microelectronic Engineering **9**, 31-36 (1989).
7. Soichi Owa and Hiroyuki Nagasaka, "Immersion lithography; its potential performance and issues," Proc. SPIE, Vol. 5040, 724 (2003).
8. Takashi Miyamatsu, Yong Wang, Motoyuki Shima, Shiro Kusumoto, Takashi Chiba, Hiroki Nakagawa, Katsuhiko Hieda, and Tsutomu Shimokawa, "Material design for immersion lithography with high refractive index fluid (HIF)," Proc. SPIE, Vol. 5753, 10 (2005).

9. D. Carter, D. Gil, R. Menon, I. Djomehri, and H. Smith, "Zone-plate array lithography (ZPAL): a new maskless approach," Proc. SPIE, Vol. 3676, 324 (1999).

10. D. Attwood, *Soft X-ray and extreme ultraviolet radiation: principle and applications* Cambridge University Press, New York, 1999.

11. J. A. Hoffnagle, W. D. Hinsberg, M. Sanchez, and F. A. Houle, "Liquid immersion deep-ultraviolet interferometric lithography," J. Vac. Sci. Technol. B **17**, 3306-3309 (1999).

12. F. Jenkins and H. White, *Fundamentals of Optics*, Fourth Edition, McGraw-Hill, New York, 1976.

13. J. W. Goodman, *Statistical Optics*, Wiley-Interscience, New York, 1985.

14. Yang-Kyu Choi, Tsu-Jae King, "A Spacer Patterning Technology for Nanoscale CMOS," IEEE Transactions on Electronic Devices **49**, 436-441 (2002).

15. Y. Ohmura, M. Nakagawa, T. Matsuyama, Y. Shibazaki, "Catadioptric lens development for DUV and VUV projection optics," Proc SPIE **5040**, 781-788 (2003).

16. D. Williamson, "Catadioptric optical reduction system with high numerical aperture," US Patent #5537260 (1996).

17. C. Rim, Y. Cho, H. Kong, S. Lee, "Four-mirror imaging system (magnification +1/5) for ArF excimer laser lithography," Opt. and Quant. Electron. **27**, 319-325 (1994).

18. Y. Zhang, D. Lu, H. Zou, Z. Wang, "Excimer laser photolithography with a 1:1 broadband catadioptric optics," Proc. SPIE **1463**, 456-463 (1991).

19. J. H Underwood and T. W. Barbee, Jr., "Layered synthetic microstructures as Bragg diffractors for X rays and extreme ultraviolet: theory and predicted performance," Appl. Opt. **20**, 3027-3034 (1981).

20. D. Brandt, et al., "LPP source system development for HVM," Proc. SPIE **7271**, 727103-727103-10 (2009).

21. A. Endo, et al., "Laser-produced plasma source development for EUV lithography," Proc. SPIE **7271**, 727108-727108-7 (2009).

22. M Yoshioka, et al., “Xenon DPP source technologies for EUVL exposure tools,” Proc. SPIE **7271**, 727109-727109-8 (2009).

23. S. Harilal, B. O'Shay, M. Tillack, “Debris mitigation in a laser-produced tin plume using a magnetic field,” J. Appl. Phys. **98**, 036102 (2005)

24. S. Fujioka, H. Nishimura, K. Nishihara, M. Murakami, Y. Kang, Q. Gu, K. Nagai, T. Norimatsu, N. Miyanaga, Y. Izawa, K. Mima, “Properties of ion debris emitted from laser-produced mass-limited tin plasmas for extreme ultraviolet light source applications,” Appl. Phys. Lett. **87**, 241503 (2005).

25. S. Namba, S. Fujioka, H. Nishimura, Y. Yasuda, K. Nagai, N. Miyanaga, Y. Izawa, K. Mima, K. Takiyama, “Spectroscopic study of debris mitigation with minimum-mass Sn laser plasma for extreme ultraviolet lithography,” Appl. Phys. Lett. **88**, 171503 (2006)

26. E. Vargas López, B. Jurczyk, M. Jaworski, M. Neumann, D. Ruzic, “Origins of debris and mitigation through a secondary RF plasma system for discharge-produced EUV sources,” Microelectron. Engin. **77**, 95-102 (2005).

27. E. Antonsen, K. Thompson, M. Hendricks, D. Alman, B. Jurczyk, D. Ruzic, “Ion debris characterization from a z-pinch extreme ultraviolet light source,” J. Appl. Phys. **99**, 063301 (2006).

28. V. Sizyuk, A. Hassanein, V. Bakshi, “Modeling and optimization of debris mitigation systems for laser and discharge-produced plasma in extreme ultraviolet lithography devices,” J. Micro/Nanolithography, MEMS and MOEMS **6**, 043003 (2007).

29. H. Oizumi, A. Izumi, K. Motai, I. Nishiyama, and A. Namiki, “Atomic Hydrogen Cleaning of Surface Ru Oxide Formed by Extreme Ultraviolet Irradiation of Ru-Capped Multilayer Mirrors in H2O Ambience,” Jap. J. of Appl. Phys. **46**, L633–L635 (2007).

30. J. M. Bennett and L. Mattson, *Introduction to Surface Roughness and Scattering*, Optical Society of America, Washington, D.C. (1989).

31. T. Miura, K. Murakami, H. Kawai, Y. Kohama, K. Morita, K. Hada, and Y. Ohkubo, “Nikon EUVL development progress update,” Proc. SPIE **7271**, 72711X (2009).

32. D. Tichenor, D. Stearns, J. Bjorkholm, E. Gullikson, S. Hector, "Compensation of flare-induced CD changes EUVL," U. S. Patent #6815129, 11/9/2004.

33. F. Schellenberg, J. Word, O. Toublan, "Layout compensation for EUV flare," Proc. SPIE **5751**, 320-329 (2005).

34. H. Meiling, H. Meijer, V. Banine, R. Moors, R. Groeneveld, H. Voorma, U. Mickan, B. Wolschrijn, B. Mertens, G. van Baars, P. Kürz, N. Harned, "First performance results of the ASML alpha demo tool," Proc. SPIE **6151**, 615108-1-12 (2006).

35. O. Wood, et al. "Integration of EUV lithography in the fabrication of 22-nm node devices," Proc. SPIE **7271**, 727104-727104-10 (2009).

36. J. Park, et al. "The application of EUV lithography for 40nm node DRAM device and beyond," Proc. SPIE **7271**, 727114-727114-8 (2009).

37. G. Vandentop, et al. "Demonstration of full-field patterning of 32 nm test chips using EUVL," Proc. SPIE **7271**, 727116-727116-9 (2009).

38. H. Meiling, et al., "Performance of the Full Field EUV Systems," Proc. SPIE **6921**, 69210L-69210L-13 (2008).

39. B. LaFontaine, et al., "The use of EUV lithography to produce demonstration devices," Proc. SPIE **6921**, 69210P-69210P-10 (2008).

40. P. Naulleau, *et al.*, "Status of EUV micro-exposure capabilities at the ALS using the 0.3-NA MET optic," Proc. SPIE **5374**, 881-891 (2004).

41. A. Brunton, *et al*., "High-resolution EUV imaging tools for resist exposure and aerial image monitoring," Proc. SPIE **5751**, 78-89 (2005).

42. P. Naulleau, C. Anderson, K. Dean, P. Denham, K. Goldberg, B. Hoef, B. La Fontaine, T. Wallow, "Recent results from the Berkeley 0.3-NA EUV microfield exposure tool," Proc. SPIE **6517**, 65170V (2007).

43. N. Nishimura, G. Takahashi, T. Tsuji, H. Morishima, S. Uzawa, "Study of system performance in SFET," Proc SPIE **6921**, (2008).

44. H. Meiling, et al. "EUVL system: moving towards production," Proc. SPIE **7271**, 727102-727102-15 (2009).

45. J. Benschop, "ASML EUV Program: Status and Prospects," 2009 International Symposium on Extreme Ultraviolet Lithography, Prague, Czech Republic, October 18-October 23, 2009, proceedings available from SEMATECH, Austin, TX.

46. T. Tsarfati, E. Zoethout, E. Louis, R. van de Kruijs, A. Yakshin, S. Müllender, F. Bijkerk, "Improved contrast and reflectivity of multilayer reflective optics for wavelengths beyond the extreme UV," Proc. SPIE **7271**, 72713V (2009).

List of figures

DISCLAIMER

This work was supported by the Director, Office of Science, of the U.S. Department of Energy under Contract No. DE-AC02-05CH11231.